


Different CT slice thickness and contrast-enhancement phase in radiomics models on the differential performance of lung adenocarcinoma

Yang Wang¹ | Fang Liu² | Yan Mo³ | Chencui Huang³ | Yingxin Chen² | Fuliang Chen⁴ | Xiangwei Zhang⁵ | Yunxin Yin⁶ | Qiang Liu¹ | Lin Zhang⁵ 

¹Department of Radiology, Shandong Provincial Hospital, Shandong University, Jinan, Shandong, China

²Department of Radiology, Shandong Provincial Hospital Affiliated to Shandong First Medical University, Jinan, Shandong, China

³Department of Research Collaboration, R&D center, Beijing Deepwise & League of PHD Technology Co., Ltd, Beijing, China

⁴Department of Thoracic Surgery, Chengxin Hospital, Yuncheng, Shandong, China

⁵Department of Thoracic Surgery, Shandong Provincial Hospital, Shandong University, Jinan, Shandong, China

⁶Department of Thoracic Surgery, Shandong Provincial Hospital Affiliated to Shandong First Medical University, Jinan, Shandong, China

Correspondence

Qiang Liu, Department of Radiology, Shandong Provincial Hospital, Shandong University, Jinan, Shandong, 250021, China.

Email: liuqiangdoc@126.com

Lin Zhang, Department of Thoracic Surgery, Shandong Provincial Hospital, Shandong University, Jinan, Shandong, 250021, China.

Email: doczhanglin@163.com

Funding information

Jinan Science and Technology Development Program, Grant/Award Number: 201907066; Shandong Province Key Research and Development Fund Program, Grant/Award Number: NO. ZR2019MH106; Research and Development

Abstract

Background: To investigate the effects of computed tomography (CT) reconstruction slice thickness and contrast-enhancement phase on the differential diagnosis performance of radiomic signature in lung adenocarcinoma.

Methods: A total of 187 patients who had been pathologically confirmed with lung adenocarcinoma and nonadenocarcinoma were divided into a training cohort ($n = 149$) and validation cohort ($n = 38$). All the patients underwent contrast-enhanced CT and the images were reconstructed with different slice thickness. The radiomic features were extracted from different slice thickness and scan phase. The logistic regression (LR) algorithm was used to build a machine learning model for each group. The area under the curve (AUC) obtained from the receiver operating characteristic (ROC) curve and DeLong test was used to evaluate its discriminating performance.

Results: Finally, 34 image features and five semantic features were selected to establish a radiomics model. Based on the three contrast-enhanced CT phases and four reconstruction slice thickness, 12 groups of radiomics models showed good discrimination ability with the AUCs range from 0.9287 to 0.9631, sensitivity range from 0.8349 to 0.9083, specificity range from 0.825 to 0.925 in the training group. Similar results were observed in the validation group. However, there was no statistical significance between the different CT scan phase groups and different slice thickness ($p > 0.05$).

Conclusions: The radiomic analysis of contrast-enhanced CT can be used for the differential diagnosis of lung adenocarcinoma. Moreover, different slice thickness and contrast-enhanced scan phase did not affect the discriminating ability in the radiomics models.

KEYWORDS

lung adenocarcinoma, radiomics, slice thickness, scan phase

Yang Wang and Fang Liu contributed equally to this work.

[Correction added on 19 May 2022, after first online publication: in the Correspondence section, Lin Zhang's address has been amended.]

[Correction added on 19 May 2022, after first online publication: the study included 187 patients who underwent contrasted chest CT that consisted 3 different scan phases (plain phase, arterial phase, and venous phase) but was described as 561 (187×3) by mistake. The values were modified in the Abstract, Methods, and Results section as well as in Table 1.]

INTRODUCTION

Lung cancer is one of the most common malignancies worldwide. The different pathological subtypes of lung cancer have distinct biological characteristics; thus, clinical treatment and prognosis also differ.¹ Adenocarcinoma is the dominant

pathological type, and targeted therapies can significantly improve the efficacy of treatment for lung adenocarcinoma.² Therefore, it is helpful to determine the histological subtype of adenocarcinoma before determining the appropriate therapeutic strategy.

With the increased uptake of low-dose computed tomography (CT) screening, an increasing number of lung lesions are being detected. CT is important for clinical decision making, but sometimes its ability to provide a differential diagnosis is limited.³ Radiomics involves the conversion of images to data of a higher dimension and subsequent mining of these data to improve decision making.⁴ Recently, radiomics studies of pulmonary lesions have differentiated benign from malignant nodules, defined the pathological type, predicted lung cancer gene mutations, determined the prognosis of lung cancer, and evaluated therapeutic efficacy. Yang et al. constructed a radiomics model to differentiate pulmonary granulomatous nodules from solid lung adenocarcinomas. With this model, radiomic features were extracted from plain-phase and venous-phase CT images with a slice thickness of 2.0 mm.⁵ Zhong et al. also constructed a radiomics model to predict occult mediastinal lymph node metastasis in lung adenocarcinoma. With this approach, radiomic features were extracted from plain CT images with a slice thickness of 1.0 mm.⁶ Moreover, Gu et al. constructed a radiomics model to predict cell proliferation (Ki-67 staining) in non-small cell lung cancer. In their study, radiomic features were extracted from plain or venous-phase CT images with a slice thickness of 5.0 mm.⁷

The major limitations of radiomics are the lack of acquisition parameter standardization, inconsistent radiomic methods, and lack of reproducibility.⁸ Although radiomics has been widely used in previous studies,^{5–7} there is still no consensus on the image parameters that should be employed to establish radiomics models. Contrast-enhanced CT images obtained in different phases (plain, arterial phase, and venous phase) and with different slice thicknesses may have different effects on the radiomics results. Therefore, the purpose of this study was to develop and validate a prediction model using radiomic features extracted from CT images to differentiate lung adenocarcinoma and to investigate the effects of reconstruction slice thickness and contrast-enhancement phase on the performance of radiomics to differentially diagnose lung adenocarcinoma.

METHODS

Patients

This retrospective study was approved by Shandong Provincial Hospital Affiliated to Shandong First Medical University. The study protocol was approved by the institutional review board of our institution. The requirement for informed patient consent was waived due to the retrospective nature of the study. We reviewed the records of 187 patients who underwent chest CT at our institution from January 2019 to December 2020. The inclusion criteria were (a) patients with

available CT images in the picture archiving and communication system; (b) patients with images that could be reconstructed; and (c) patients in whom lung lesions were examined pathologically. The exclusion criteria were (a) patients who underwent treatment before CT and (b) patients with intrapulmonary metastases.

CT image acquisition

All patients underwent contrast-enhanced CT of the entire thorax. CT examinations were performed using a Toshiba 640-slice CT scanner and the GE Flash 256-slice CT scanner. The scanning parameters were as follows: tube rotation time, 0.75/0.5 s; pitch, 0.9; detector collimation, 128 × 0.625; tube voltage, 120 kV; tube current, 160–300 mA; field of view, 350 mm; matrix, 512 × 512; reconstruction interval, 1 mm; convolution kernel, B; slice thickness, 1 mm and 2 mm; voxel spacing (X and Y directions), 0.68–0.87 mm. Images were normalized to isometric voxels (1 mm) using cubic interpolation. All of the original images (plain-phase, arterial-phase, and venous-phase images) were reconstructed with a standard convolution kernel at four slice thicknesses (0.5, 1.0, 2.0, and 3.0 mm).

Region of interest segmentation

Twelve groups of images were uploaded to the Deepwise multimodal research platform (<https://keyan.deepwise.com>, V1.6.2) in Digital Imaging and Communications in Medicine format for region of interest (ROI) segmentation, semantic feature annotation, and further radiomic analysis.⁸ The lesions were segmented in each CT slice by a radiologist with more than 10 years of CT imaging experience. The lesions were segmented manually to obtain the ROI according to the following rule: the ROI should include the full lesion region, including the lesion edges, and avoid the peripheral blood vessels, pleura, atelectasis, and cavity if possible. Figure 1 demonstrates the ROI delineations of two patients, one with adenocarcinoma and one without adenocarcinoma. The semantic features were as follows: (1) lobulated sign (no lobulated sign, shallow lobulated sign, deep lobulated sign), (2) maximum diameter (diameter ≤ 1.0 cm, 1.0 cm < diameter ≤ 3.0 cm, diameter > 3.0 cm), (3) spiculated sign (no spiculated sign, short spiculated sign, long spiculated sign), (4) pleural indentation (no pleural indentation, pleural indentation), (5) lesion density (pure ground-glass nodules, mixed ground-glass nodules, solid nodules) and (6) pathological type (adenocarcinoma, nonadenocarcinoma).

Radiomics research

Image preprocessing

According to the ROI labeled by the radiologist in the original CT images, we used the B-spline interpolation sampling

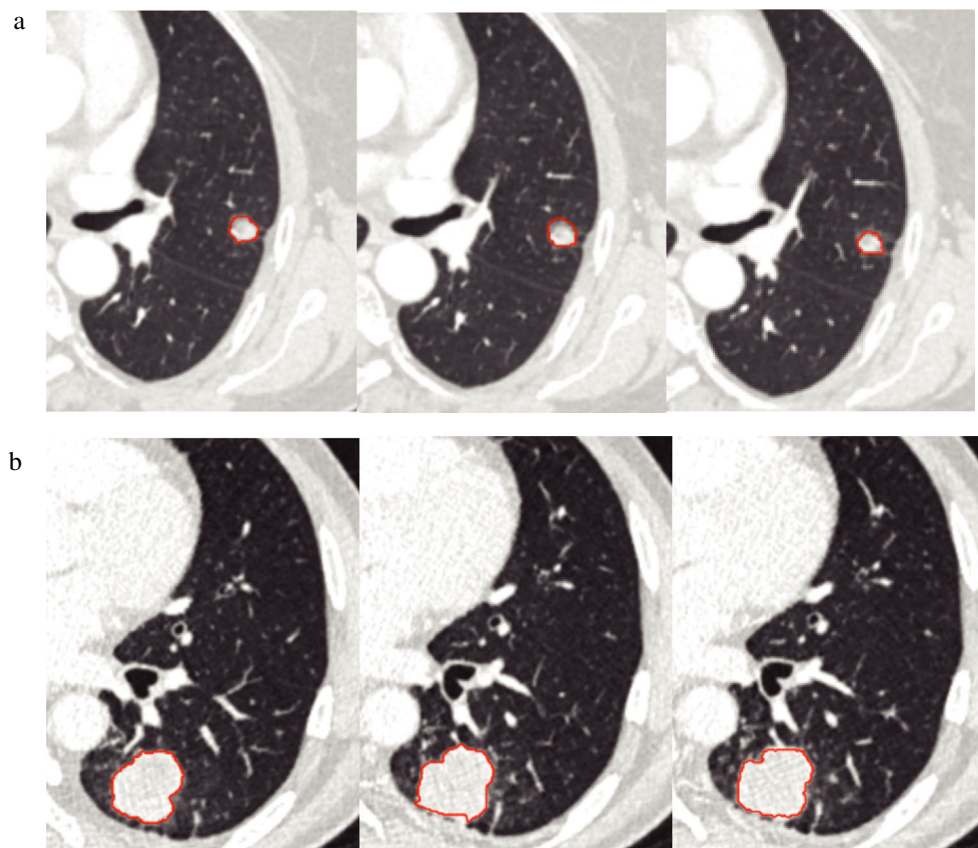


FIGURE 1 The receiver-operating characteristics (ROI) delineations for two patients respectively. One patient (a) was diagnosed with adenocarcinoma and another patient (b) was diagnosed with nonadenocarcinoma.

technique to resample the images with different resolutions to guarantee that all of the images had the same resolution after resampling to [1,1,1].⁹ Different methods (LoG, Sigma, Wavelet, Square, SquareRoot, Logarithm, Exponential, Gradient, LBP2D) were used for image transformation.¹⁰

Feature extraction and quantification

To obtain stable image features, we performed preliminary feature selection. First, we examined the intraobserver reproducibility of radiomic features with 30 randomly chosen patients to exclude human error caused by multiple labeling. The same radiologist repeated ROI segmentation twice at an interval of 1 week. The image features of each delineated ROI were measured and recorded, and the intraclass correlation coefficients (ICCs) were calculated.^{11,12} Features with an ICC >0.9 were retained. Then, the Pearson's correlation coefficients of these features were calculated, and the features with correlation coefficients <0.9 were retained for further feature selection. Second, we summarized the semantic features and retained the CT radiomic features. We used the F-test for feature selection and two sets of data to calculate the sample standard deviation of the square. We then calculated the sample standard deviation of the two groups of data of square (F value <https://statisticsbyjim.com/anova/f-tests-anova/>). We compared the calculated F value with the F value in the table; if the calculated F value was less than the F value from the table, no significant difference between

the two groups was concluded. Finally, we retained 10% of the imaging radiomic features to construct clinical semantic imaging radiomics models.

The radiomic features of the transformed images were extracted,¹³ including first-order features based on the pixel values of the original image or the preprocessed image; the features describing the lesion shape; and the features describing the internal and surface texture of the lesion, including the gray level co-occurrence matrix, the gray level run length matrix, the gray level size zone matrix, and the gray level dependence matrix (<https://pyradiomics.readthedocs.io/en/latest/features.html>).

Finally, a total of 1 648 radiomic features were extracted from each ROI and standardized using the Z-score.¹⁴ Feature extraction was performed using PyRadiomics, which is a comprehensive open-source platform that enables the processing and extraction of radiomic features from medical images and is implemented in Python.

Constructing the radiomics model

All datasets were randomly split and divided into the training cohort and the validation cohort at a ratio of 7:3. Machine learning models for the identification of adenocarcinoma and nonadenocarcinoma were constructed, and the models were evaluated and compared.

The influence of contrast-enhanced CT phases and slice thicknesses on the differentiation of adenocarcinoma and

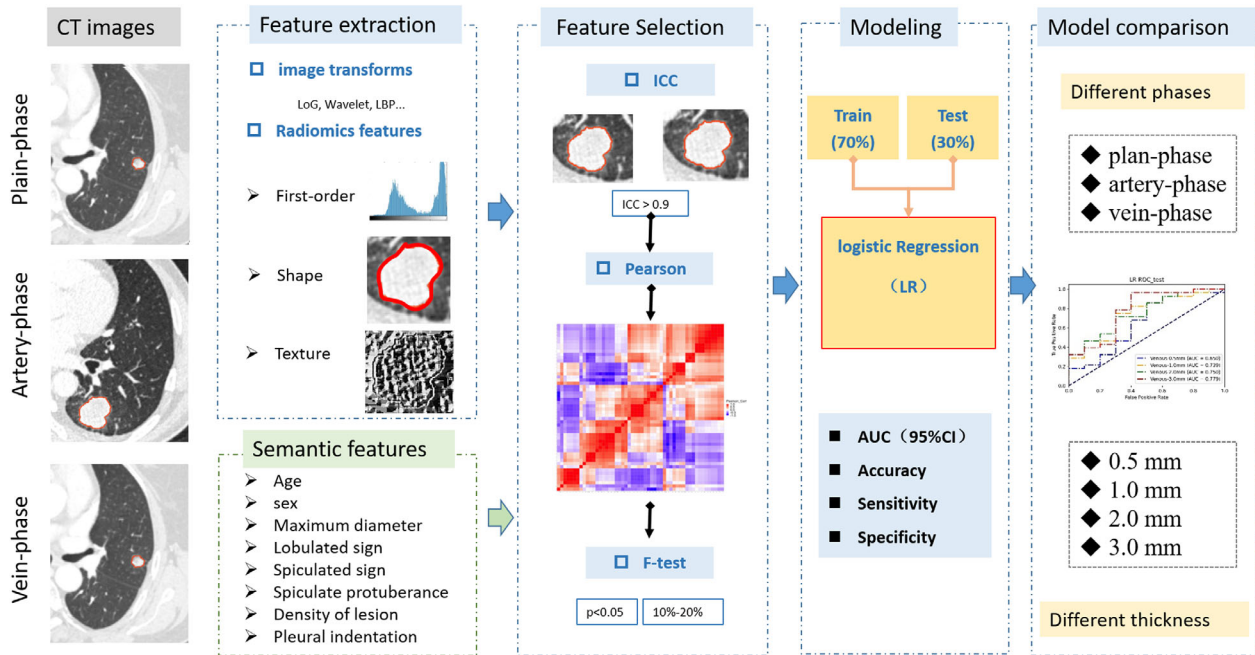


FIGURE 2 The radiomic analysis workflow

nonadenocarcinoma was evaluated by constructing radiomics models. In the training stage, we used the global super parameter search method to traverse different parameter settings for feature filtering. Eleven simple and integrated machine learning algorithms,¹⁵ including LogisticRegression, SVM, LinearSVC, DecisionTree, RandomForest, AdaBoost, GradientBoosting, XGBoost, BernoulliNB, GaussianNB, and KNearestNeighbors, were evaluated for their classification performance in the training and test sets, and the area under the curve (AUC), accuracy, sensitivity, specificity, and number of modeling features were compared.

Finally, we used the logistic regression (LR) algorithm to build 12 machine learning classifiers representing the 12 sets of chest CT images with different imaging parameters, as follows: plain phase, 0.5 mm (P0.5); plain phase, 1.0 mm (P1.0); plain phase, 2.0 mm (P2.0); plain phase, 3.0 mm (P3.0); arterial phase, 0.5 mm (A0.5); arterial phase, 1.0 mm (A1.0); arterial phase, 2.0 mm (A2.0); arterial phase, 3.0 mm (A3.0); venous phase, 0.5 mm (V0.5); venous phase, 1.0 mm (V1.0); venous phase, 2.0 mm (V2.0); venous phase, 3.0 mm (V3.0). The above 12 models were compared and discussed in detail according to different CT thicknesses and phases. Figure 2 shows the radiomic analysis workflow.

Statistical analysis

Based on R and the Deepwise DxAI platform (<https://dxonline.deepwise.com>), the mean, frequency, and percentage were used to describe variables. When differences between groups were analyzed, the independent-samples *t*-test was used for normally distributed numerical variables, while the chi-square test was used for categorical variables.

Receiver operating characteristic (ROC) curves were constructed using Python. The AUC, accuracy, sensitivity, and specificity were used to describe the classification performance of the different models, and the DeLong test was used to determine whether differences in the AUC between models were significant.¹⁶ In the bilateral significance test, a *p*-value < 0.05 was considered statistically significant.

RESULTS

Patient characteristics

A total of 187 patients with lung lesions were included in this study. Patient characteristics and lung lesions characteristics are provided in Table 1. There were significant differences between the nonadenocarcinoma and adenocarcinoma groups in most of the semantic features (maximum diameter, lobulated sign, lesion density, and pleural indentation) and sex (*p* < 0.05 for all).

Radiomics models

For each ROI in each image group, 1 648 image features and five semantic features were extracted. We removed 149 features with intraobserver instability according to the ICC, as well as 1 300 highly linearly correlated features according to Pearson's correlation coefficient (>0.9). We retained 365 features for feature selection and machine learning. Using the homogeneity test of variance, we used 34 image features and five semantic features to construct the logistic regression models, and the performance of each model was evaluated.

TABLE 1 Distribution of patients and lung lesions characteristics

	Patients (<i>n</i> = 187)		<i>p</i> -value
	Nonadenocarcinoma (<i>n</i> = 50)	Adenocarcinoma (<i>n</i> = 137)	
Age (year ± SD)	58.04 ± 12.357	57.036 ± 9.896	0.355 ^a
Sex			0.001 ^b
Female	16 (32.0%)	81 (59.1%)	
Male	34 (68.0%)	56 (40.9%)	
Maximum diameter (cm)			0.003 ^b
$d \leq 1.0$	13 (26.0%)	27 (19.7%)	
$1 < d < 3$	22 (44.0%)	94 (68.6%)	
$d > 3$	15 (30.0%)	16 (11.7%)	
Lobulated sign			<0.001 ^b
No	7 (14.0%)	1 (0.7%)	
Shallow	30 (60.0%)	71 (51.8%)	
Deep	13 (26.0%)	65 (47.4%)	
Spiculated sign			0.083 ^b
No	35 (70.0%)	75 (54.7%)	
Short	13 (26.0%)	43 (31.4%)	
Long	2 (4.0%)	19 (13.9%)	
Density of lesion			<0.001 ^b
pGGO	2 (4.0%)	23 (16.8%)	
mGGO	9 (18.0%)	68 (49.6%)	
Solid nodules	39 (78.0%)	46 (33.6%)	
Plural indentation			<0.001 ^b
No	32 (64.0%)	62 (45.3%)	
Stripe	10 (20.0%)	2 (1.5%)	
Yes	8 (16.0%)	73 (53.3%)	

Abbreviations: SD, standard deviation; mGGO, mixed ground-glass opacity; pGGO, pure ground-glass opacity.

^aIndependent samples *t*-test.

^bChi-square test/calibration Chi-square test.

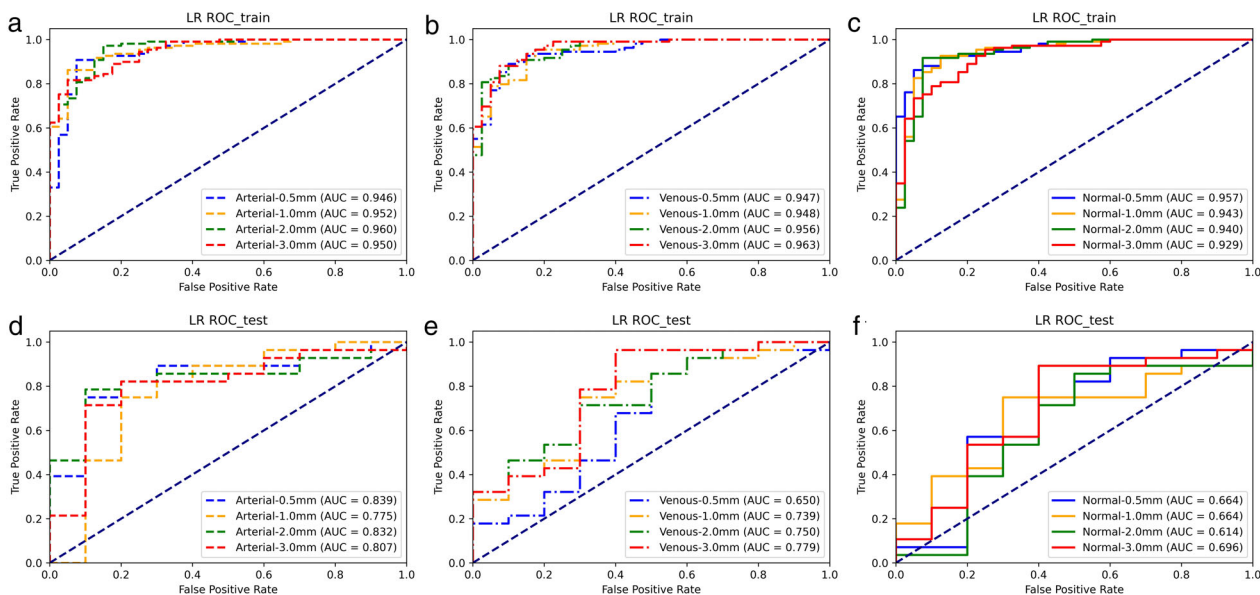


FIGURE 3 The receiver-operating characteristics (ROC) curve in each group. Different slice thickness in arterial phase (a), venous phase (b) and normal phase (c) of the training cohorts. Different slice thickness in arterial phase (d), venous phase (e) and normal phase (f) of the validation cohorts

TABLE 2 The model performances of the training cohort

	Plain-phase	Artery-phase	Vein-phase
LR - 0.5 mm			
AUC (95% CI)	0.9571	0.9459	0.9466
Accuracy	0.8926	0.8792	0.8926
Sensitivity	0.8807	0.8624	0.8899
Specificity	0.925	0.925	0.9
LR - 1.0 mm			
AUC (95% CI)	0.9433	0.9521	0.9479
Accuracy	0.8859	0.8792	0.8658
Sensitivity	0.8899	0.8807	0.8716
Specificity	0.875	0.875	0.85
LR - 2.0 mm			
AUC (95% CI)	0.9397	0.9601	0.9555
Accuracy	0.9128	0.8725	0.8792
Sensitivity	0.9083	0.8716	0.8807
Specificity	0.925	0.875	0.875
LR - 3.0 mm			
AUC (95% CI)	0.9287	0.95	0.9631
Accuracy	0.8322	0.8389	0.8859
Sensitivity	0.8349	0.844	0.8807
Specificity	0.825	0.825	0.9

Abbreviations: LR, logistic regression; AUC, area under curve; CI, confidence interval.

TABLE 3 The model performances of the validation cohort

	Plain-phase	Artery-phase	Vein-phase
LR - 0.5 mm			
AUC (95% CI)	0.6643	0.8393	0.65
Accuracy	0.6316	0.8158	0.7368
Sensitivity	0.6429	0.8571	0.8214
Specificity	0.6	0.7	0.5
LR - 1.0 mm			
AUC (95% CI)	0.6643	0.775	0.7393
Accuracy	0.7105	0.7632	0.7105
Sensitivity	0.7143	0.8214	0.75
Specificity	0.7	0.6	0.6
LR - 2.0 mm			
AUC (95% CI)	0.6143	0.8321	0.75
Accuracy	0.7632	0.8158	0.7105
Sensitivity	0.8571	0.8214	0.7857
Specificity	0.5	0.8	0.5
LR - 3.0 mm			
AUC (95% CI)	0.6964	0.8071	0.7786
Accuracy	0.7105	0.7895	0.7632
Sensitivity	0.75	0.7857	0.8214
Specificity	0.6	0.8	0.6

Abbreviations: LR, logistic regression; AUC, area under curve; CI, confidence interval.

TABLE 4 The *p*-value results comparing the difference in AUC of receiver-operating characteristic (ROC) between groups,

	Training cohort	Validation cohort
0.5 mm slice thickness		
A0.5 mm vs. V0.5 mm	0.9631	0.027
A0.5 mm vs. P0.5 mm	0.3895	0.0727
V0.5 mm vs. P0.5 mm	0.4410	0.8800
1.0 mm slice thickness		
A1.0 mm vs. V1.0 mm	0.7127	0.6746
A1.0 mm vs. P1.0 mm	0.4894	0.2165
V1.0 mm vs. P1.0 mm	0.7287	0.2260
2.0 mm slice thickness		
A2.0 mm vs. V2.0 mm	0.7007	0.2961
A2.0 mm vs. P2.0 mm	0.2035	0.0574
V2.0 mm vs. P2.0 mm	0.4302	0.1564
3.0 mm slice thickness		
A3.0 mm vs. V3.0 mm	0.2471	0.7186
A3.0 mm vs. P3.0 mm	0.1955	0.1377
V3.0 mm vs. P3.0 mm	0.0148	0.1606
Artery-phase		
A0.5 mm vs. A1.0 mm	0.6343	0.2949
A0.5 mm vs. A2.0 mm	0.1976	0.9194
A0.5 mm vs. A3.0 mm	0.7771	0.7564
A1.0 mm vs. A2.0 mm	0.5016	0.5957
A1.0 mm vs. A3.0 mm	0.8637	0.8063
A2.0 mm vs. A3.0 mm	0.3960	0.7767
Vein-phase		
V0.5 mm vs. V1.0 mm	0.9228	0.0789
V0.5 mm vs. V2.0 mm	0.4429	0.2717
V0.5 mm vs. V3.0 mm	0.1909	0.1640
V1.0 mm vs. V2.0 mm	0.5954	0.8877
V1.0 mm vs. V3.0 mm	0.2160	0.6169
V2.0 mm vs. V3.0 mm	0.4820	0.6050
Plain-phase		
P0.5 mm vs. P1.0 mm	0.3061	1.0000
P0.5 mm vs. P2.0 mm	0.3232	0.4872
P0.5 mm vs. P3.0 mm	0.0705	0.7563
P1.0 mm vs. P2.0 mm	0.7684	0.4578
P1.0 mm vs. P3.0 mm	0.2617	0.6994
P2.0 mm vs. P3.0 mm	0.4209	0.4355

Note: $p < 0.05$ was statistically significant (Delong test)

Abbreviations: ROC, receiver operating characteristic; AUC, area under curve; A, artery-phase; V, vein-phase; P, plain-phase.

The ROC curves of the training and validation cohorts in each group are shown in Figure 3, and the model performances are summarized in Tables 2 and 3. The DeLong test was used to compare the AUC of the ROC curve between the two groups, and the results are summarized in Table 4.

As shown in Tables 2–4, in the training cohort, when comparing the four slice thicknesses in the plain-phase group (P0.5, P1.0, P2.0, and P3.0), the maximum AUC was

observed in the P0.5 group (AUC: 0.9571 vs. 0.9433 vs. 0.9397 vs. 0.9287, respectively); however, there were no significant differences between the four slice thicknesses ($p > 0.05$). When comparing the slice thicknesses in the arterial-phase group (A0.5, A1.0, A2.0, A3.0), the maximum AUC was observed in the A2.0 group (AUC: 0.9459 vs. 0.9521 vs. 0.9601 vs. 0.950, respectively); however, there were no significant differences ($p > 0.05$). In the venous-phase group (V0.5, V1.0, V2.0, V3.0), the maximum AUC was observed in the V3.0 group (AUC: 0.9466 vs. 0.9479 vs. 0.9555 vs. 0.9631, respectively); however, no significant differences were noted ($p > 0.05$). Although the AUCs of the four slice thicknesses differed within one CT scan phase, no statistically significant differences were noted.

When comparing the CT scan phases, in the 0.5-mm slice thickness group (P0.5, A0.5, V0.5), the maximum AUC was observed in the P0.5 group (0.9571). In the 1.0-mm slice thickness group (P1.0, A1.0, V1.0), the maximum AUC was observed in the V1.0 group (0.9521); in the 2.0-mm slice thickness group (P2.0, A2.0, V2.0), the maximum AUC was observed in the A2.0 group (0.9601); and in the 3.0-mm slice thickness group (P3.0, A3.0, V3.0), the maximum AUC was observed in the V3.0 group (0.9631). No statistically significant differences were observed ($p > 0.05$). The same observations were made in the validation cohort.

DISCUSSION

Radiomics is used to diagnose pulmonary lesions, but the reproducibility of published research is poor, and widespread clinical application has been limited, possibly because of the lack of standardized image acquisition and quality control approaches. The consensus among researchers is that thin slices are beneficial to display the details of lesions when performing pulmonary lesion radiomics; however, the signal-to-noise ratio of CT images is significantly reduced with the reduction in CT image layer thickness. Consequently, quantitative feature extraction is affected, and the diagnostic efficiency of the radiomics model is reduced.¹⁷ It will be necessary to provide standards for images used in radiomics if the field is to realize its potential.

Our study constructed radiomics models for 12 groups of CT images in three dynamic contrast-enhanced CT phases (plain-phase, arterial-phase, and venous-phase CT) and at four slice thicknesses (0.5, 1.0, 2.0, and 3.0 mm) for the differential diagnosis of adenocarcinoma and non-adenocarcinoma. The diagnostic performance of these approaches was compared with the DeLong test. The results demonstrated no significant difference between groups within one phase with different slice thicknesses. Moreover, there was no significant difference between groups within one slice thickness in different phases. In addition, the training cohort of 12 radiomics models showed high diagnostic efficiency with a minimum AUC of 0.9287 and a maximum AUC of 0.9631. The AUC values in the validation cohort were generally lower than the AUC values in the training

cohort, probably because of the small sample size. Overall, this study demonstrated that the phase of dynamic contrast-enhanced CT and the thickness of chest CT images had no significant effect on the efficacy of the radiomics models.

Li et al. constructed a radiomics model to predict epidermal growth factor receptor mutation status in primary lung adenocarcinoma using two slice thicknesses (thin: 1 mm; thick: 5 mm). In their study, the prediction model that used thin slices (1 mm) was better than the prediction model that used thick slices (5 mm), and the effect of the convolution kernel was not significant.¹⁸ He et al. constructed a radiomics model to discriminate benign and malignant solitary pulmonary nodules using noncontrast and contrast-enhanced CT images and two reconstruction slice thicknesses (thin: 1.25 mm; thick: 5 mm). The results demonstrated that the radiomic signature acquired with noncontrast-enhanced CT, thin slices, and the standard convolution kernel was better for the differential diagnosis of solitary pulmonary nodules.¹⁹ Compared with the present study, the difference between the layer thicknesses used in each of these studies (4.0 and 3.75 mm, respectively) was greater than in the present study, and the maximum layer thickness (5.0 mm) was greater than in our study. Our study used four slice thicknesses (0.5, 1.0, 2.0, and 3.0 mm), and the difference between these slice thicknesses was smaller, with a maximum slice thickness of 3.0 mm. The results demonstrated that compared with the 3.0-mm slice thickness, a thickness of less than 3.0 mm (0.5, 1.0, or 2.0 mm) did not significantly improve the diagnostic performance of the radiomics models. Therefore, there is no need to choose a thinner CT image slice thickness to construct pulmonary lesion radiomics models, because thinner slices will increase the workload of researchers in terms of ROI segmentation, as well as the storage load of the images.

He et al. demonstrated that a radiomic signature based on noncontrast-enhanced CT images showed better performance in the differential diagnosis of solitary pulmonary nodules than a radiomic signature based on contrast-enhanced CT images.¹⁹ The underlying reason may be that the biological heterogeneity within the tumor that can be depicted by radiomic features may be confounded by intravenous injection of contrast material; however, this conclusion is not consistent with our study. Although different phases of dynamic contrast-enhanced CT have been used in previous studies,^{5–7,20} most of the studies obtained a positive prediction result. Combined with the results of our study, these results show no significant difference between the groups within one slice thickness with different phases. This suggests that researchers could select plain-phase CT images to construct pulmonary lesion radiomics models, which would reduce the complexity of image acquisition, as well as the financial burden on patients.

The goal of radiomics is to convert images into mineable high-fidelity and high-throughput data.²¹ A radiomics study can be structured in five phases: data selection, medical imaging, feature extraction, exploratory analysis, and modeling, each with its own challenges. Standardization of acquisition parameters using consistent radiomics methods and improving their reproducibility across multiple sites are

important for classification model validation.⁸ Furthermore, human-machine-assisted interpretation studies are needed to explore how the use of radiomics alongside radiologists will improve diagnostic accuracy, reduce costs by decreasing the need for further testing, and decrease the time that radiologists spend performing scans.²² We designed this study from a clinical perspective to explore the potential CT image criteria. The results suggest a simplified and economical method for CT image selection in radiomics studies.

Our study has some limitations that should be noted. First, the sample size in this study was small. Further large-sample studies are needed to improve the accuracy of the results. Second, we did not group the lesions according to the lesion diameter. For lesions smaller than 1 cm in diameter, it will be important to determine whether the predictive performance of the radiomics models significantly improves when using a thinner slice thickness. In future studies, we will arrange pulmonary lesions into groups based on their maximum diameter. Third, this study was internally validated, and all patients attended the same hospital; thus, external validation will be needed to improve the credibility and reproducibility of the model.²³

In conclusion, our study demonstrated that the radiomic analysis of contrast-enhanced CT images can be used for the differential diagnosis of lung adenocarcinoma. Moreover, the radiomic signature built based on 12 groups of CT images showed no significant differences. Different slice thicknesses and contrast-enhanced CT scan phases did not affect the discriminative ability of the radiomics model. Thus, clinicians may choose plain-phase CT with an adequate slice thickness to establish the radiomics-based database for chest CT. However, the results need to be confirmed in prospective, randomized, multicenter clinical trials with larger sample sizes.

ACKNOWLEDGMENTS

The work was supported by Shandong Province Key Research and Development Fund Program: no. ZR2019MH106; Jinan Science and Technology Development Program, grant/award no: 201907066.

CONFLICT OF INTEREST

The authors confirm that there are no conflicts of interest.

ORCID

Lin Zhang  <https://orcid.org/0000-0003-1187-1015>

REFERENCES

- Bade BC, Dela Cruz CS. Lung cancer 2020: epidemiology, etiology, and prevention. *Clin Chest Med*. 2020;41(1):1–24.
- Travis WD, Brambilla E, Nicholson AG, Yatabe Y, Austin JHM, Beasley MB, et al. The 2015 world health organization classification of lung tumors: impact of genetic, clinical and radiologic advances since the 2004 classification. *J Thorac Oncol*. 2015;10(9):1243–60.
- Aberle DR, Adams AM, Berg CD, Black WC, Clapp JD, Fagerstrom RM, et al. Reduced lung-cancer mortality with low-dose computed tomographic screening. *N Engl J Med*. 2011;365(5):395–409.
- Gillies RJ, Kinahan PE, Hricak H. Radiomics: images are more than pictures, they are data. *Radiology*. 2016;278(2):563–77.
- Yang X, He J, Wang J, Li W, Liu C, Gao D, et al. CT-based radiomics signature for differentiating solitary granulomatous nodules from solid lung adenocarcinoma. *Lung Cancer*. 2018;125:109–14.
- Zhong Y, Yuan M, Zhang T, Zhang YD, Li H, Yu TF. Radiomics approach to prediction of occult mediastinal lymph node metastasis of lung adenocarcinoma. *AJR Am J Roentgenol*. 2018;211(1):109–13.
- Gu Q, Feng Z, Liang Q, Li M, Deng J, Ma M, et al. Machine learning-based radiomics strategy for prediction of cell proliferation in non-small cell lung cancer. *Eur J Radiol*. 2019;118:32–7.
- Thawani R, McLane M, Beig N, Ghose S, Prasanna P, Velcheti V, et al. Radiomics and radiogenomics in lung cancer: a review for the clinician. *Lung Cancer*. 2018;115:34–41.
- M. Svoboda LM-I, F. M. Frigura-Iliasa and P. Andea. B-spline interpolation technique for digital signal processing. 2015 International Conference on Information and Digital Technologies. 2015:366–71.
- Gonzalez RCWRE. Digital image processing. *IEEE Trans Acoust Speech Signal Process*. 1977;28(4):484–6.
- Romeo V, Cavaliere C, Imbriaco M, Verde F, Petretta M, Franzese M, et al. Tumor segmentation analysis at different post-contrast time points: a possible source of variability of quantitative DCE-MRI parameters in locally advanced breast cancer. *Eur J Radiol*. 2020;126:108907.
- Shrout PE, Fleiss JL. Intraclass correlations: uses in assessing rater reliability. *Psychol Bull*. 1979;86(2):420–8.
- Zwanenburg A, Vallières M, Abdalah MA, Aerts H, Andrearczyk V, Apte A, et al. The image biomarker standardization initiative: standardized quantitative Radiomics for high-throughput image-based phenotyping. *Radiology*. 2020;295(2):328–38.
- Friston KJ, Ashburner J, Frith CD, Poline J-B, Heather JD, Frackowiak RSJ. Spatial registration and normalization of images. *Hum Brain Mapp*. 1995;3(3):165–89.
- Mitchell TM. Machine learning (international editions). The McGraw-Hill Companies, Inc., Beijing: China Machine Press; 2003.
- DeLong ER, DeLong DM, Clarke-Pearson DL. Comparing the areas under two or more correlated receiver operating characteristic curves: a nonparametric approach. *Biometrics*. 1988;44(3):837–45.
- Lee KB, Goo HW. Quantitative image quality and histogram-based evaluations of an iterative reconstruction algorithm at low-to-ultralow radiation dose levels: a phantom study in chest CT. *Korean J Radiol*. 2018;19(1):119–29.
- Li Y, Lu L, Xiao M, Dercle L, Huang Y, Zhang Z, et al. CT slice thickness and convolution kernel affect performance of a Radiomic model for predicting EGFR status in non-small cell lung cancer: a preliminary study. *Sci Rep*. 2018;8(1):17913.
- He L, Huang Y, Ma Z, Liang C, Liang C, Liu Z. Effects of contrast-enhancement, reconstruction slice thickness and convolution kernel on the diagnostic performance of radiomics signature in solitary pulmonary nodule. *Sci Rep*. 2016;6:34921.
- Chae HD, Park CM, Park SJ, Lee SM, Kim KG, Goo JM. Computerized texture analysis of persistent part-solid ground-glass nodules: differentiation of preinvasive lesions from invasive pulmonary adenocarcinomas. *Radiology*. 2014;273(1):285–93.
- Kumar V, Gu Y, Basu S, Berglund A, Eschrich SA, Schabath MB, et al. Radiomics: the process and the challenges. *Magn Reson Imaging*. 2012;30(9):1234–48.
- Wei K, Su H, Zhou G, Zhang R, Cai P, Fan Y, et al. Potential application of Radiomics for differentiating solitary pulmonary nodules. *OMICS J Radiol*. 2016;5(2):1000218.
- Lambin P, Leijenaar RTH, Deist TM, Peerlings J, de Jong EEC, van Timmeren J, et al. Radiomics: the bridge between medical imaging and personalized medicine. *Nat Rev Clin Oncol*. 2017;14(12):749–62.

How to cite this article: Wang Y, Liu F, Mo Y, Huang C, Chen Y, Chen F, et al. Different CT slice thickness and contrast-enhancement phase in radiomics models on the differential performance of lung adenocarcinoma. *Thorac Cancer*. 2022;13(12):1806–13. <https://doi.org/10.1111/1759-7714.14459>